

NONRIGID POINT CORRESPONDENCE RECOVERY FOR PLANAR CURVES USING FOURIER DECOMPOSITION

Min Li, Chandra Kambhamettu

Video/Image Modeling and Synthesis Lab
Department of Computer and Information Sciences
University of Delaware
Newark, DE 19716 USA
mli/chandra@cis.udel.edu

ABSTRACT

A novel method of point correspondence recovery between planar curves is presented in this paper where motion between the curves is nonrigid. Fourier transformation is used to decompose planar curves into a set of ellipses, each at a different frequency level. The point correspondences between two planar curves is based on the correspondences between two ellipses in the same frequency level. At each level, a simple method is implemented to get the correspondences between the two ellipses through their shape information. This way, nonrigid point correspondence problem between two planar curves is decomposed to a set of simple subproblems – the correspondence between ellipses. We have conducted comprehensive experiments on synthetic and real data sets and found that the algorithm is quite effective and efficient.

1. INTRODUCTION

1.1. Related Work

Correspondence recovery is an important step in many computer vision applications. Given the object's structure captured in two time instances, it is critical to recover the point correspondence between these two structures for understanding the motion of the object. Motion of many real world objects is usually nonrigid and involves arbitrary (unknown model) deformation which makes the correspondence recovery difficult.

One way to overcome the difficulty is to constrain the deformation type. An explicit motion model is usually utilized in these methods. This motion model simplifies the nonrigid motion and its parameters can be solved by local searching for a pair of points that best fit the predefined motion model [9][2]. The motion types are limited in these methods. Many researchers also recover the correspondence from the shape information. This can be accomplished implicitly by optimizing an objective function.

In [1] [6], matching is achieved by minimizing a curvature based bending energy. Wang [15] introduced a matching method by defining an error function which combines Euclidean distance, surface normal and curvature. Local searching is necessary for these methods to find the best matching which minimizes the objective function.

Correspondence recovery is also a common task in surface registration problem. Correspondence between two surfaces will guide the registration process and the registration result will in turn decide the correspondence between two surfaces. To accomplish these two tasks simultaneously, iterative algorithms are proposed in [4][7] [16][5]. In each iteration, an objective function is minimized according to the current recovered correspondence and motion between the two surfaces is resolved. This motion will bring two surfaces towards each other and a new correspondence will be decided according to some criterion. This new correspondence is then used to recover a better motion in the next iteration.

In [14], two problems of using curvature and objective function for nonrigid correspondence recovery are pointed out by Tagare. First, minimization of pure curvature difference for nonrigid motion estimation will be problematic since the curvature is only a rigid invariant. Second, the objective functions are not guaranteed to be symmetric with respect to the two surfaces being compared. The above problems can be avoided by directly comparing the geometry of two shapes. Belongie [3] matches two shapes by comparing the point shape context which is a set of points around the point of interest. This method is suitable for objects with certain shapes and it is designed for object recognition. It can not be applied to the analysis of nonrigid motion of closed curves.

To describe shapes of closed curves, elliptic Fourier decomposition has been widely used in computer vision [13][11] [10] for segmentation and object recognition. The parameter space warping (PSW) [12] method introduced by Meier

also uses elliptic Fourier decomposition for correspondence recovery but two shapes are still compared with the rigid invariants such as curvature and surface normal. Our proposed method not only decomposes the object shape but also decomposes the motion between two closed curves. At each level, the decomposition of motion is decided directly by the geometry of decomposed shapes. Recovered correspondence is guaranteed to be symmetric because switching the “before” and “after” motion curves does not effect the resulting correspondence.

1.2. General Approach

Our approach of matching is similar to the parameter space warping (PSW) technique[12]. Correspondence between two objects is defined as the mapping of parameter between the objects. PSW finds the best parameter mapping by a global search in the parameter space while our approach gets the parameter mapping directly from the geometry of objects. In our approach, the problem of correspondence recovery between two objects is divided into a set of sub-problems, i.e, correspondence between ellipses.

A closed contour can be represented using a parametric description by the following Fourier transformation:

$$\vec{x}(t) = \sum_k \vec{e}_k(k, t) = \sum_k \vec{a}_k \vec{B}_k(t). \quad (1)$$

B_k is the basis function, a_k is the coefficients for level k and t is the parameter, usually defined as the polar angle. Vector $\vec{x}(t)$ is the Cartesian object coordinates. It is modeled as a superposition of vector \vec{e}_k . As we will explain in the next section, \vec{e}_k represents an ellipse in geometry.

Using Equation(1), two object boundaries (planar contours) can be described by sets of ellipses at different levels. At each level, correspondence between the two ellipses will give us partial information about the correspondence between the two object contours. Information collected from all the levels gives us the mapping relationship between the two objects. Thus, similar to the Fourier transformation which decomposes a shape into simple shapes, we decompose the correspondence mapping between the two shapes to simple parameter mappings.

There are three main steps in this correspondence recovery approach: 1) decomposing both object boundaries to sets of ellipses in different levels, 2) estimation of parameter mapping between the ellipse pairs in each level, 3) composing of parameter mapping of all the levels into a final parameter mapping between the two object contours. The process is shown in Figure 1.

2. SHAPE DECOMPOSITION

The boundaries of organs, cells and other biomedical objects usually can be represented by closed curves. The elliptic Fourier representation of a closed curve is[13][11][10]:

$$\begin{bmatrix} x(t) \\ y(t) \end{bmatrix} = \begin{bmatrix} a_0 \\ c_0 \end{bmatrix} + \sum_{k=1}^{\infty} \begin{bmatrix} a_k & b_k \\ c_k & d_k \end{bmatrix} \begin{bmatrix} \cos(kt) \\ \sin(kt) \end{bmatrix} \quad (2)$$

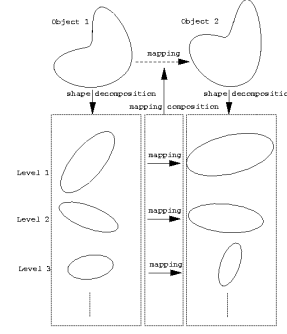


Fig. 1. General approach: 1) Shape decomposition. 2) Parameter mapping between ellipses. 3) Parameter mapping composition.

where

$$\begin{aligned} a_0 &= \frac{1}{2\pi} \int_0^{2\pi} x(t) dt & c_0 &= \frac{1}{2\pi} \int_0^{2\pi} y(t) dt \\ a_k &= \frac{1}{2\pi} \int_0^{2\pi} x(t) \cos(kt) dt & b_k &= \frac{1}{2\pi} \int_0^{2\pi} x(t) \sin(kt) dt \\ c_k &= \frac{1}{2\pi} \int_0^{2\pi} y(t) \cos(kt) dt & d_k &= \frac{1}{2\pi} \int_0^{2\pi} y(t) \sin(kt) dt. \end{aligned} \quad (3)$$

From geometry perspective, (a_0, c_0) is the center of the closed curve and

$$\begin{bmatrix} x_k(t) \\ y_k(t) \end{bmatrix} = \begin{bmatrix} a_k & b_k \\ c_k & d_k \end{bmatrix} \begin{bmatrix} \cos(kt) \\ \sin(kt) \end{bmatrix} \quad (4)$$

is an ellipse. we call it the k^{th} ellipse of the closed curve $(x(t), y(t))$. The center of the k^{th} ellipse is $(0, 0)$ but its semi-major axis and semi-minor axis are usually not aligned with the x and y axes. The phase shift of the k^{th} ellipse is also not 0 in general. To describe the shape of this ellipse, it is necessary to know the semi-major axis length, the semi-minor axis length and phase shift value. Mathematically, the Equation(4) can be written as:

$$\begin{bmatrix} x_k(t) \\ y_k(t) \end{bmatrix} = r_k \begin{bmatrix} A_k & 0 \\ 0 & B_k \end{bmatrix} p_k \begin{bmatrix} \cos(kt) \\ \sin(kt) \end{bmatrix} \quad (5)$$

where

$$r_k = \begin{bmatrix} \cos \theta_k & -\sin \theta_k \\ \sin \theta_k & \cos \theta_k \end{bmatrix} \quad p_k = \begin{bmatrix} \cos \phi_k & -\sin \phi_k \\ \sin \phi_k & \cos \phi_k \end{bmatrix}. \quad (6)$$

Other parts of Equation(5) can be used to define a standard ellipse

$$\begin{bmatrix} x_k^{std}(u) \\ y_k^{std}(u) \end{bmatrix} = \begin{bmatrix} A_k & 0 \\ 0 & B_k \end{bmatrix} \begin{bmatrix} \cos(u) \\ \sin(u) \end{bmatrix} \quad (7)$$

where $u = kt$.

From Equation (5) and (7), it can be seen that r_k defines a rotation and p_k defines a phase shift between the k^{th}

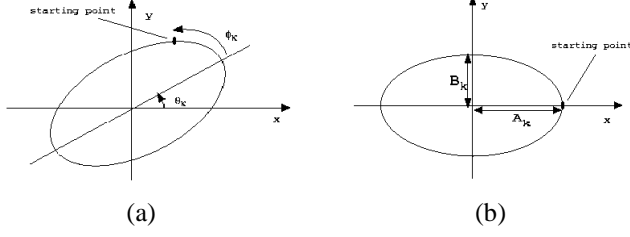


Fig. 2. (a) The k^{th} ellipse. (b) The standard ellipse.

ellipse and a standard ellipse. The values of rotation and phase shift are θ_k and ϕ_k respectively. It is also clear that these two ellipses have same semi-major axis length A_k and same semi-minor axis length B_k . Figure 2 shows the relationship between these two ellipses.

The following equations are given by [13]:

$$\begin{aligned} A_k^2 &= \frac{\alpha + \sqrt{\alpha^2 - 4\beta^2}}{2} & B_k^2 &= \frac{2\beta^2}{\alpha + \sqrt{\alpha^2 - 4\beta^2}} \\ \theta_k &= \tan^{-1} \frac{A_k c_k + B_k b_k}{A_k a_k - B_k d_k} & \phi_k &= \tan^{-1} \frac{B_k a_k - A_k d_k}{A_k c_k + B_k b_k} \end{aligned} \quad (8)$$

where

$$\alpha = a_k^2 + b_k^2 + c_k^2 + d_k^2, \beta = a_k d_k - b_k c_k. \quad (9)$$

3. PARAMETER MAPPING

Given a before-motion curve $(x(t), y(t))$ and an after-motion curve $(x'(t'), y'(t'))$, the problem of finding corresponding point in the after-motion curve for every point in the before-motion curve can be solved if the mapping from t to t' is known. That is, for a point with parameter t in the before-motion curve, we need to know the parameter t' of its corresponding point in the after-motion curve. Formally, for a pair of corresponding points, the mapping between their parameters is:

$$\Delta t(t) = t' - t \quad (10)$$

and Δt for every point $(x(t), y(t))$ is needed to solve the correspondence problem.

From Equations (2) and (4), one can see that a closed curve can be decomposed into a set of ellipses. The shape of the curve is decided by the shapes of ellipses in different levels. As the correspondence between the two curves depend on their shape, it is natural to seek the correspondences between the decomposed ellipse pairs at each level. Thus Δt , the mapping from t to t' , can be decomposed to a set of values, Δt_k , where Δt_k is the mapping from t to t' in the k^{th} level and the mapping should be decided by the shapes of these two k^{th} level ellipses.

Given the k^{th} level ellipse \vec{e}_k of the before-motion curve and the k^{th} level ellipse \vec{e}'_k of the after-motion curve, the semi-major axis lengths and semi-minor axis lengths of \vec{e}_k

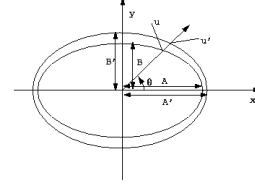


Fig. 3. Correspondence between two ellipses

and \vec{e}'_k are A_k, B_k and A'_k, B'_k respectively. If A_k is close to A'_k and B_k is close to B'_k , we say these two ellipses are similar. By rotating \vec{e}_k and \vec{e}'_k with angles $-\theta_k$ and $-\theta'_k$ respectively (θ_k is defined in Equation(8)) we will overlay the rotated ellipses with their standard ellipses and these rotations will not change the ellipse shapes. Shape comparison between \vec{e}_k and \vec{e}'_k can then be done by comparing their standard ellipses.

If the orientation of \vec{e}_k is counterclockwise, a point in \vec{e}_k with parameter t will have parameter u in the standard ellipse $x_k(u) = A_k \cos u, y_k(u) = B_k \sin u$ ($0 \leq u \leq 2\pi$) after the rotation. The relationship between t and u is:

$$u = kt + \phi_k \text{ mod } 2\pi. \quad (11)$$

The point in \vec{e}'_k with parameter t' can be dealt with in the same way. After the rotation, it will be located to a point with parameter u' in the standard ellipse $x'_k(u') = A'_k \cos u', y'_k(u') = B'_k \sin u'$ ($0 \leq u' \leq 2\pi$) and

$$u' = kt' + \phi'_k \text{ mod } 2\pi. \quad (12)$$

A simple point correspondence recovery method for similar standard ellipses is shown in Figure 3. Two points are corresponding to each other if they have the same polar angle θ . For a standard ellipse defined in Equation(7), the angle of a point has relationship with its parameter u as:

$$\theta = \tan^{-1} \left(\frac{B_k}{A_k} \tan u \right). \quad (13)$$

Then the mapping from u to u' (u and u' have the same polar angle of θ) between these two ellipse is

$$\Delta u_k(u) = u' - u = \tan^{-1} \left(\frac{A'_k B_k}{A_k B'_k} \tan u \right) - u. \quad (14)$$

From Equations (11), (12) and (14), the parameter mapping $\Delta t_k(t) = kt' - kt$ between two k^{th} level ellipses can be decided. The parameter mapping between the two object contours will be solved if all $\Delta t_k(t)$ in different levels are composed to a single mapping $\Delta t(t)$. In practice, the number of decomposed levels must have an upper limit H ; i.e., a curve $(x(t), y(t))$ is approximated by H ellipses. The majority shape information is encoded at the lower frequency

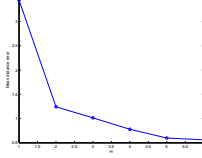


Fig. 4. The recovery error is decreased when the number of total frequency levels involved is increased.

levels and increasing H will give a more accurate description of the curve shape. Therefore, the mapping from t to t' in lower frequency levels contributes more to the overall mapping.

Based on above observations, for two curves $(x(t), y(t))$ and $(x'(t'), y'(t'))$ which are approximated by H ellipses respectively, we define the mapping between their parameters by composing parameter mapping from level 1 to H :

$$\Delta t(t) = \frac{\sum_{k=1}^H \frac{\Delta t_k(t)}{k}}{H}. \quad (15)$$

This definition combines information from different levels and gives more credits to the lower levels. When the number of total levels is increased, it should give more accurate mapping between two contours. This can be seen from Figure 4 in which 6 frequency levels are used to recover the point correspondence between two curves and the recovery error is decreased when the number of total frequency levels involved is increased. These two curves and the deformation between them are shown in the first row and first column of Figure 5. More details about the experiment are presented in Section 6.1.

4. MAPPING INVARIANCE

Equation(15) defines the correspondence between two curves according to the correspondence information from ellipses. The correspondence recovery in our framework is based on the shape and thus invariant to rigid transformation and the parameterization start point. The translation component in our case only changes the geometry center and keeps all decomposed ellipses untouched. The effect of rotation and parameterization starting point difference is discussed below.

4.1. Rotation

After Rotating curve $(x(t), y(t))$ by an angle θ , its k^{th} level ellipse will be:

$$\begin{bmatrix} x_k^\theta(t) \\ y_k^\theta(t) \end{bmatrix} = r_k^\theta \begin{bmatrix} A_k & 0 \\ 0 & B_k \end{bmatrix} p_k \begin{bmatrix} \cos(kt) \\ \sin(kt) \end{bmatrix} \quad (16)$$

where $r_k^\theta = R \cdot r_k$ and

$$R = \begin{bmatrix} \cos \theta & -\sin \theta \\ \sin \theta & \cos \theta \end{bmatrix} \quad (17)$$

is the rotation matrix. One can see that after a rotation the shape of the k^{th} level ellipse is not changed and only the angle between the k^{th} level ellipse and its standard ellipse has been changed. This change will not affect our correspondence recovery.

4.2. Starting Point

If the parameterization starting point of curve $(x(t), y(t))$ is displaced by a value λ , this curve can be written as $(x^\lambda(t^\lambda), y^\lambda(t^\lambda))$ which is the same curve as $(x(t), y(t))$ except that it has a different parameter t^λ . The new parameter t^λ and the original parameter t has the relationship:

$$t = t^\lambda + \lambda. \quad (18)$$

The k^{th} level ellipse \vec{e}_k^λ of the same curve with new parameter t^λ is:

$$\begin{bmatrix} x_k^\lambda(t^\lambda) \\ y_k^\lambda(t^\lambda) \end{bmatrix} = \begin{bmatrix} a_k^\lambda & b_k^\lambda \\ c_k^\lambda & d_k^\lambda \end{bmatrix} \begin{bmatrix} \cos(kt^\lambda) \\ \sin(kt^\lambda) \end{bmatrix}. \quad (19)$$

\vec{e}_k^λ has the same shape as the original k^{th} level ellipse \vec{e}_k ; i.e, they correspond to the same standard ellipse. But \vec{e}_k^λ has an additional phase shift $k\lambda$ compared with \vec{e}_k [11][10]. Then in the k^{th} level, compared with the original mapping Δt the new mapping Δt^λ is:

$$\Delta t_k^\lambda(t^\lambda) = \Delta t_k(t) - k\lambda. \quad (20)$$

Substitute Equation (20) into Equation (15), we get:

$$\Delta t^\lambda(t^\lambda) = \Delta t(t) - \lambda. \quad (21)$$

Thus, a displacement λ of the parameterization starting point gives a displacement λ in the recovered parameter mapping.

5. IMPLEMENTATION

To decide the upper limit H of decomposed ellipse levels, we compare the similarity between two k^{th} level ellipses of the before-motion and after-motion curves. Define $r_k = A_k/B_k$ and $r'_k = A'_k/B'_k$. If $r_k/r'_k \leq \gamma$ where γ is a threshold, the k^{th} level is taken into account for the parameter mapping. In general, ellipses of before-motion and after-motion curves are similar in some low levels and they are different to each other when the level is high.

6. EXPERIMENTS AND ANALYSIS

6.1. Synthetic Data

After a shape template is chosen, two different nonrigid transformations are used to warp it to its corresponding after-motion curve. The first transformation we applied is an affine motion. The second transformation we used is the Gaussian Radial Basis Function (GRBF) [8], so that more complex nonrigid deformation is presented between the before-motion and after-motion curves. The coefficients of the GRBF were sampled from a Gaussian distribution with zero

	Shape 1	Shape 2	Shape 3
Affine	0.62	0.93	0.81
GRBF	0.81	1.36	1.57

Table 1. Mean distance errors(in pixels) of the synthetic experiment.

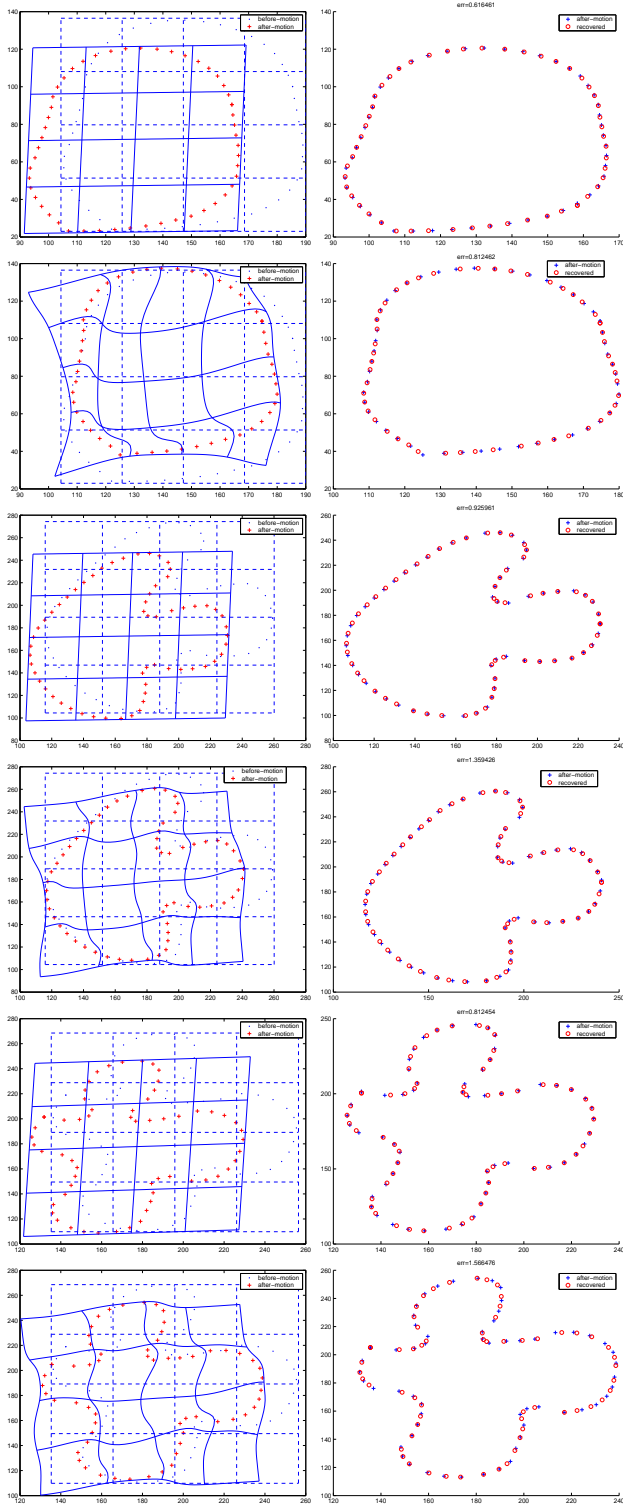


Fig. 5. Synthetic experiments on 3 different shapes. See Section 6.1 for details

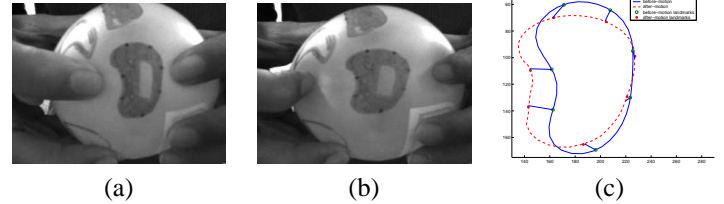


Fig. 6. First experiment on real motion. (a)Before stretching. (b)After stretching. (c)Recovered correspondence, circles and stars are landmarks.

mean. The error is defined as the mean distance between the recovered corresponding points and the true corresponding points in the warped(after-motion) curve.

Three shapes are shown in the synthetic experiment. The first curve is a relatively simple shape and the last two are more irregular. The results are shown in Figure 5. Every two rows in Figure 5 belong to the experiments on one shape. For each shape, the first row is the affine transformation and the second row is the GRBF transformation. Each row has two parts. The left part shows the shape template(dot) and its warped curve(cross). The deformation is also shown in this part. The right part is the comparison between the recovered correspondence points(circle) and the true corresponding points(cross) in the warped shape. Table 1 lists the recovery errors of all synthetic experiments.

6.2. Real Nonrigid Motion

Our method has also been tested on shapes undergoing real nonrigid motion. In the first experiment, the shape is a character "D" on the surface of a balloon and the motion is created by stretching the balloon around the shape unevenly. The "D" shape before and after stretching is shown in Figure 6(a) and (b) respectively. The boundary of the shape is extracted with a parametrically deformable model [13] which will give us the necessary Fourier parameters directly after the boundary finding. Seven landmarks along the shape edge are manually drawn on the balloon surface to supply reliable correspondence information. For each landmark point in the before-stretching image, the distance between the recovered corresponding point and the true corresponding landmark in the after-motion image is calculated. The mean value of all 7 distance errors is then used to verify the recovery result. The shapes and recovered correspondences of 7 landmarks are shown in Figure 6(c). Circles and stars in this figure are landmarks. The mean distance error here

Experiments	1	2	3
Recovery Error	1.58	1.61	1.12

Table 2. Mean distance errors(in pixels) of the experiments on real nonrigid motion.

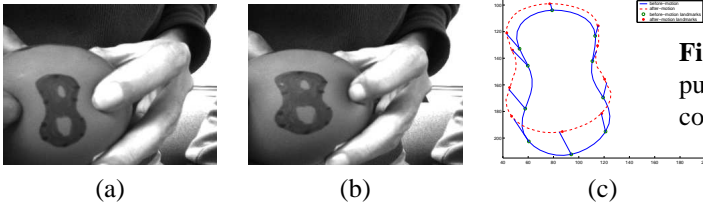


Fig. 7. The second experiment on real motion. (a)Before stretching. (b)After stretching. (c)Landmarks and recovered correspondence.

is estimated as 1.58 pixels.

The change of the "D" shape is not only caused by the imposed nonrigid motion but also by the projective distortion of the camera. Images in Figure 6 are scaled, hence the visual nonrigid motion between shapes may look smaller than what is actually imposed. But the shape difference is still obvious in Figure 6.

The second and third experiments on real motion are shown in Figures 7 and 8 respectively. Motions for these two experiments are created by stretching a balloon and pushing a ball respectively. The correspondence recovery errors for all three experiments are shown in Table 2 from which we can see the correspondence recovery errors are very less and comparable to the image resolution.

7. DISCUSSION AND FUTURE WORK

A novel method for point correspondence recovery between closed planar contours is proposed in this paper. Although we have achieved a low pixel error in the point correspondence estimation in our experiments, a better but still simple correspondence recovery algorithm between ellipse will surely improve the proposed method. More importantly, improvement of the heuristic about the composition of mappings from different Fourier frequency levels will contribute more to the proposed framework.

References

[1] A.A. Amini and J.S. Duncan. Pointwise tracking of left-ventricular motion in 3d. In *MOTION91*, pages 294–299, 1991.

[2] A.A. Amini and J.S. Duncan. Bending and stretching models for lv wall motion analysis from curves and surfaces. *IVC*, 10(6):418–430, 1992.

[3] S. Belongie, J. Malik, and J. Puzicha. Matching shapes. In *ICCV01*, pages I: 454–461, 2001.

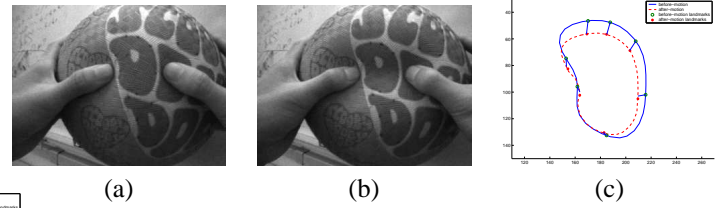


Fig. 8. The third experiment on real motion. (a)Before pushing. (b)After pushing. (c)Landmarks and recovered correspondence.

[4] P.J. Besl and N.D. McKay. A method for registration of 3-d shapes. *PAMI*, 14(2):239–256, February 1992.

[5] H. Chui and A. Rangarajan. A new algorithm for non-rigid point matching. In *CVPR00*, pages II:44–51, 2000.

[6] J.S. Duncan, R.L. Owen, L.H. Staib, and P. Anandan. Measurement of non-rigid motion using contour shape descriptors. In *CVPR91*, pages 318–324, 1991.

[7] J. Feldmar and N.J. Ayache. Rigid, affine and locally affine registration of free-form surfaces. *IJCV*, 18(2):99–119, May 1996.

[8] M. Fornefett, K. Rohr, and H.S. Stiehl. Elastic registration of medical images using radial basis functions with compact support. In *CVPR99*, pages I: 402–407, 1999.

[9] C. Kambhamettu and D.B. Goldgof. Curvature-based approach to point correspondence recovery in conformal nonrigid motion. *CVGIP*, 60(1):26–43, July 1994.

[10] F.P. Kuhl and C.R. Giardina. Elliptic fourier features of a closed contour. *Computer Graphics and Image Processing*, (18):236–258, 1982.

[11] C.S. Lin and C.L. Hwang. New forms of shape invariants from elliptic fourier descriptors'. *Pattern Recognition*, 20(5):535–545, 1987.

[12] D. Meier and E. Fisher. Parameter space warping: Shape-based correspondence between morphologically different objects. *MedImg*, 21(1):31–47, January 2002.

[13] L.H. Staib and J.S. Duncan. Boundary finding with parametrically deformable models. *PAMI*, 14(11):1061–1075, November 1992.

[14] H.D. Tagare. Shape-based nonrigid correspondence with application to heart motion analysis. *MedImg*, 18(7):570–579, July 1999.

[15] Y. Wang, B.S. Peterson, and L.H. Staib. Shape-based 3d surface correspondence using geodesics and local geometry. In *CVPR00*, pages II:644–651, 2000.

[16] Z.Y. Zhang. Iterative point matching for registration of free-form curves and surfaces. *IJCV*, 13(2):119–152, October 1994.